Published in: Langmuir 24:16 (2008) 8841-8849

Inverted Microcontact Printing on Polystyrene-*block*-Poly(*tert*-butyl acrylate) Films: A Versatile Approach to Fabricate Structured Biointerfaces Across the Length Scales

Anika Embrechts,[1] Chuan Liang Feng,[1,&] Christopher A. Mills,[2] Michael Lee,[2] Ilona Bredebusch,[3] Jürgen Schnekenburger,[3] Wolfram Domschke,[3] G. Julius Vancso,[1] and Holger Schönherr[1,*]

1 University of Twente, MESA$^+$ Institute for Nanotechnology and Faculty of Science and Technology, Department of Materials Science and Technology of Polymers, P.O. Box 217, 7500 AE Enschede, The Netherlands

2 Nanobioengineering group, Institute for Bioengineering of Catalonia (IBEC), Barcelona Science Park, Josep Samitier 1-5, 08028 Barcelona, Spain.

3 Gastroenterologische Molekulare Zellbiologie, Medizinische Klinik und Poliklinik B, Westfälische Wilhelms-Universität, Domagkstr. 3A, 48149 Münster, Germany

& Current address: Max-Planck-Institute for Polymer Research, Ackermannweg 10, 55128 Mainz, Germany

* corresponding author: e-mail: h.schonherr@tnw.utwente.nl;

tel.: ++31 53 489 3170; fax.: ++31 53 489 3823

Published in: Langmuir 24:16 (2008) 8841-8849

Abstract

The combination of the recently introduced soft lithographic technique of *inverted microcontact printing (i-μCP)* and spin-coated films of polystyrene-*block*-poly(*tert*-butyl acrylate) (PS_{690}-b-$PtBA_{1210}$) as a reactive platform is shown to yield a versatile approach for the facile fabrication of topographically structured and chemically patterned biointerfaces with characteristic spacings and distances that cross many orders of magnitude. The shortcomings of conventional μCP in printing of small features with large spacings, due to the collapse of small or high aspect ratio stamp structures, are circumvented in i-μCP by printing reactants using a featureless elastomeric stamp onto a topographically structured reactive polymer film. Prior to molecular transfer, the substrate-supported PS_{690}-b-$PtBA_{1210}$ films were structured by imprint lithography resulting in lateral and vertical feature sizes between > 50 μm - 150 nm and > 1.0 μm - 18 nm, respectively. Time-of-flight secondary ion mass spectrometry (ToF-SIMS) and water contact angle measurements provided evidence for the absence of surface chemical transformations during the imprinting step. Following the previously established hydrolysis and activation protocol with trifluoroacetic acid and *N*-hydroxy-succinimide, amino end-functionalized poly(ethylene glycol) ($PEGNH_2$), as well as bovine serum albumin and fibronectin as model proteins, were successfully transferred by i-μCP and coupled *covalently*. As shown, i-μCP yields increased PEG coverages and thus improved performance in suppressing non-specific adsorption of proteins by exploiting the high local concentrations in the micro- and nanocontacts during molecular transfer. The i-μCP strategy provides access to versatile biointerface platforms patterned across the length scales, as shown for guided cancer cell adhesion, which opens the pathway for systematic cell – surface interaction studies.

Introduction

For the design and fabrication of advanced biosensors[1,2] and for the study of cell-surface interactions[3,4,5] biochemical patterning and topographical structuring on a broad range of length scales are required. These length scales are defined by the size of individual sensing elements in array-based sensor formats and the size of biological entities, such as cells and bacteria on the one hand,[5] and important biomacromolecules, including proteins and protein clusters,[6,7,8,9] on the other hand. As micro- and nanopatterns also play an important role in many other areas, their fabrication, in particular in a massively parallel manner, has attracted a great deal of attention in the past decade.[10]

In the context of functional biointerfaces,[11] suitable patterning methods must enable one to pattern larger surface areas in a parallel manner and to achieve control over surface (bio)chemical composition down to the sub-100 nm size regime together with control over topographical features and substrate modulus.[3] In addition to established optical lithographic techniques,[12] the desired patterns for functional biointerfaces can be obtained using so-called soft lithographic methods,[13,14] as well as imprinting approaches.[15]

The transfer of low molar mass molecules[13] or the direct transfer of biomolecules[14a] from a micropatterned elastomer to suitable substrates has been introduced under the terminus microcontact printing (μCP).[16] This technique has provided access to micrometer and sub-micrometer sized patterns of self-assembled monolayers, as well as biomolecules. Patterns composed of up to 16 different proteins were reported.[14a,17] Despite this success, a number of factors, such as the deformation (or collapse) of the soft elastomeric stamps[18,19] or the diffusion of ink molecules,[20,21] limit the general applicability of this approach for obtaining patterns on the 100 nm size

range. Thus new approaches must be developed or existing approaches must be refined.

Featureless stamps have been reported, among others, by the groups of Textor[22] and Huskens[23] as a means to improve conventional μCP approaches. The methodology of 'inverted microcontact printing' (i-μCP) was first applied by the group of Textor to microfabricate micrometer-sized wells of defined chemical character for single cell studies.[22] However, the authors noted that repeated stamping of the well-known poly(L-lysine)-poly(ethylene glycol) (PLL-PEG) graft copolymers[24] was required to achieve acceptable passivation. A very similar strategy was also very recently utilized by Charest et al. in a combined nanoimprint / μCP approach using a complex multistep fabrication involving the evaporation of a metal film and printing of thiols. However, as noted, low molar mass thiols are prone to infidelity of the pattern transfer on the mentioned length scales due to surface diffusion.[25]

Huskens and co-workers employed chemically patterned flat stamps among others to improve the mechanical stability of the stamp pattern and to eliminate diffusion of ink molecules via the gas phase.[23] The application of featureless stamps was also recently reported by Soolaman and Yu.[26]

We have recently introduced *reactive* microcontact printing as a versatile (soft) lithographic technique for the fabrication of patterned bio-functional interfacial architectures based on polymers for applications, such as biosensors or cell-surface interaction studies.[27] The internal structure of the block copolymer films of PS_{690}-b-$PtBA_{1210}$ with microphase separated PS cylinders and a skin layer of reactive PtBA exposed at the film surface can be exploited to obtain very robust biointerfaces. This process comprises the localized acid-catalyzed deprotection of the tBA groups, N-*hydroxy-succinimide* (NHS) activation and covalent grafting of various functionalities.[28] Thereby patterns down to the 300 nm size range were fabricated.[29]

Owing to the glassy nature of PS and the covalent amide linkages, the derivatized films showed excellent stability under a broad range of processing conditions. The combination of these polymer platforms with i-μCP would provide access to topographic structures by imprinting approaches, as well as controllable surface chemistry and high coverages of passivating (e.g. PEG) and active species (e.g., proteins and DNA) via established wet chemical conjugation strategies.[30]

As shown in this paper, i-μCP on the block copolymer-based reactive thin film platforms introduced above (Scheme 1) was developed as a methodology for the fabrication of tailored patterned biointerfaces. Owing to the absence of topographical structures in the elastomeric stamp, as well as the glassy nature of the pre-structured polymer films comprising PS microdomains, this combined approach represents a versatile method to obtain robust patterned substrates with > 10 μm down to sub-micrometer pattern sizes. In addition, the covalent amide linkages formed between the acrylate moieties of the block copolymer film and transferred molecular species in the conformal stamp-film contact result in surface modification with improved efficiency and functionality for advanced biointerface platforms.

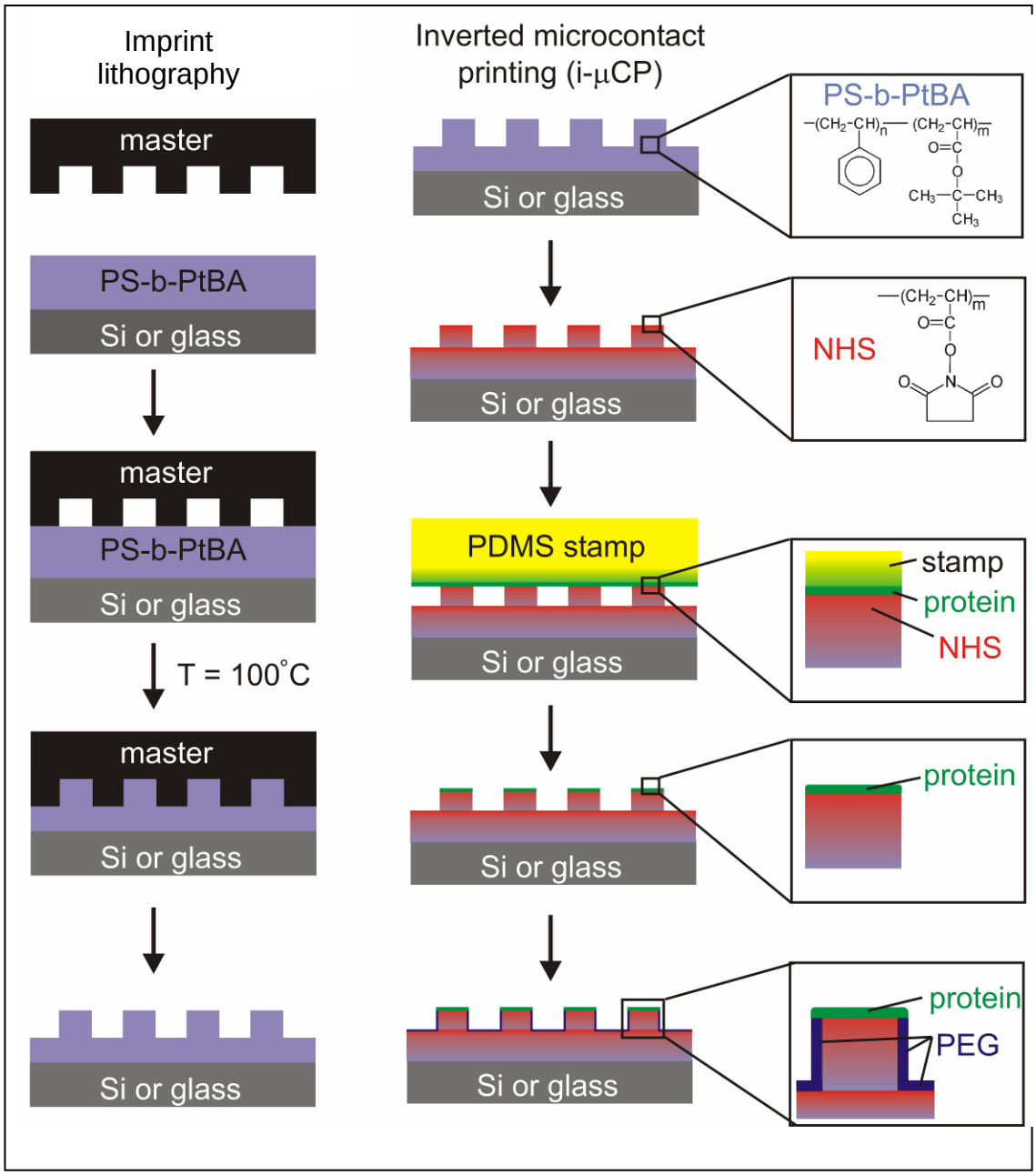

Scheme 1. Schematic of the imprint lithography (left) and reactive microcontact printing steps (middle) of the i-μCP process. The PtBA skin layer exposed at the topographically structured block copolymer film surface is hydrolyzed using TFA and subsequently activated with N-(3-dimethylaminopropyl)-N′-ethylcarbodiimide (EDC) / NHS. A hydrated protein can be transferred in the micro- or nanocontact between the oxidized elastomeric PDMS stamp and the structured film resulting in covalent attachment. In a subsequent step the non-contacted areas are passivated by covalently coupling PEG-NH_2 from buffered solution.

Experimental Section

Materials. PS_{690}-b-$PtBA_{1210}$ diblock copolymers (M_w = 202.4 kg/mol, polydispersity index (PDI) 1.03) were purchased from Polymer Source Company (Dorval, Canada) and were used as received. Amino functionalized-labeled PEG (denoted as PEG_n-NH_2) was purchased from Nektar UK Company (M_n = 500, 2000 or 5000 g/mol, PDI = 1.1). Bovine serum albumin (BSA) with Alexa Fluor-594 conjugate was bought from Molecular Probes Inc. (Breda, The Netherlands), fibronectin was purchased from Roche Diagnostics GmbH (Penzberg, Germany). Trifluoro acetic acid (TFA) and *N*-hydroxysuccinimide (NHS) were purchased from Sigma-Aldrich (Steinheim, Germany, purity ≥ 98 %). *N*-(3-Dimethylaminopropyl)-*N′*-ethylcarbodiimide hydrochloride (EDC) was purchased from Fluka (Steinheim, Germany, purity ≥ 98 %). EDC and NHS were stored at – 20 ^{o}C. Phosphate buffer saline tablets (Sigma-Aldrich, Steinheim, Germany) were used to prepare phosphate buffered saline (pH 7.4, ionic strength = 0.1397 M). Silicon (111) wafers (Okmetric N/P (100) wafers, thickness 381 ± 15 μm) or glass cover slides (Menzel-Glaser, Braunschweig, Germany) were used as substrates. These substrates were cleaned prior to use by an oxygen plasma treatment (pressure of O_2: 0.5 Bar; current: 30 mA) using an Elektrotech twin system PF 340 apparatus or a SPI Plasma Prep™ Plasma Cleaner (Structure Probe Inc, West Chester, USA). Alternatively, the substrates were cleaned in piranha solution (solution of 1:3 (v/v) 30% H_2O_2 and concentrated H_2SO_4) for 15 min and then rinsed with copious amounts of high-purity water (Millipore Milli-Q water). *Caution*: *Piranha solution should be handled with extreme caution*; *it has been reported to detonate unexpectedly.*

Film Preparation. Thin films were prepared by spin coating polymer solutions in toluene (conc. between 14 and 100 mg/mL) onto oxygen plasma or piranha-cleaned silicon wafers or glass substrates. The samples were spun at 1000 rpm for 1 s, followed

by spinning at 3000 rpm for 29 s using a P6700 spin coater (Specialty Coating Systems Inc). All spin-coated samples were annealed for 24 hours at 135°C in vacuum before analysis. Film thicknesses of 90 ± 5 nm to 1000 ± 50 nm were determined by ellipsometry (see below).

Mould fabrication.[31] Moulds for nanoimprint lithography were produced on thermally oxidized silicon wafers coated by chemical vapor-deposited silicon nitride (Si_3N_4).[32] An anti-adhesion monolayer of trichloro(tridecafluoro octyl)silane rendered the surface hydrophobic, as assessed by measurements of the advancing water contact angle (H_2O, 3 μl). The pristine Si_3N_4 produced an advancing contact angle of 73°; with the alkylsilane monolayer deposited, the surface became more hydrophobic with a contact angle of 112°.

Imprint lithography.[31] Polymer films were imprinted using PDMS stamps according to literature procedures.[22] Nanoimprinting of the polymer films was performed in a commercially available 2.5 inch nanoimprinter (Obducat AB, Sweden). In order to determine the faithfulness of the replication process, both the moulds and the nanoimprinted polymeric samples were characterized using optical microscopy (Eclipse L150, Nikon Instruments, Japan), interferometric microscopy (WYKO NT1100, Veeco, USA), scanning electron microscopy (SEM, Strata DB235; FEI Co., Netherlands), as well as AFM (see below).

Hydrolysis. The structured polymer films were hydrolyzed at room temperature in neat TFA for 15 min. All hydrolyzed films were rinsed three times thoroughly using Milli-Q water and were finally dried in a stream of nitrogen.

Activation of Hydrolyzed Polymer Films. The hydrolyzed polymer films were activated by immersion in an aqueous solution of EDC (1 M) and NHS (0.2 M) for 30

min. The samples were then rinsed with Milli-Q water, dried in a stream of nitrogen, and used immediately thereafter.

Immobilization of (Bio)Molecules on Activated Polymer Films by i-μCP. For the subsequent patterning of proteins an UV-ozone oxidized stamp[33] was immersed in BSA or fibronectin solution (1.0×10^{-4} M in PBS) for 1 hour. The stamp was then thoroughly rinsed and dried in a stream of nitrogen. Subsequently the stamp was applied to the functionalized polymer film for 30 minutes and carefully removed. Finally, the sample was rinsed with PB buffer and Milli-Q water followed by drying in a stream of nitrogen. Patterning of PEG was performed using the same procedure as mentioned above (1.0×10^{-4} M PEG-NH_2 in PBS), employing a typical stamp-substrate contact time of 3 hours unless mentioned in the text. An enhanced loading of the stamp with PEG was achieved by repeated application of drops of 1.0×10^{-4} M PEG solution in PBS followed by partial drying.

Ellipsometry. The measurements were performed with a Plasmos SD2002 instrument (rotating analyzer method) with a wavelength λ = 632.8 nm and an incidence angle equal to 70°. Film thicknesses were determined before and during sample processing on the corresponding samples that were placed in a vacuum oven for 2 hours at room temperature before the experiments were performed (to prevent water uptake by the PEG from the environment). Layer thicknesses were determined using a 2-layer model. The first layer consists of the substrate, the second layer consists of PS-b-PtBA or, after treatment, PS-b-PtBA with PEG. For the Si substrate layer a refractive index of 3.865 and an absorption coefficient of k = -0.019 were used and depending on the top layer the refractive index of PS-b-PtBA or PEG (PS-b-PtBA: 1.513, PEG: 1.4638[34]). A mean squared error (MSE) method was employed to quantify the difference between experimental and calculated model data. The Marquardt-Levenberg algorithm[35] was

applied to determine the best fit. Mean layer thicknesses and errors were determined by averaging the data from measurements performed at ten different spots on the surface.

AFM.[31] The moulds were characterized by AFM measurements using an Asylum Research MFP-3D with MikroMasch NSC18-F tips. Force – volume (FV) measurements were performed with silicon nitrides probes (Model NP, Veeco Nano Probe, Santa Barbara, CA) in air on a NanoScope IIIa multimode and a NanoScope PicoForce AFM (Digital Instruments / Veeco, Santa Barbara, CA) using cantilevers with nominal spring constant of 0.06 N/m. Height, width and period of the features observed in AFM images of the moulds were determined by analyzing cross-sectional plots. The arithmetic mean of the corresponding distance of multiple features and data points, respectively, were calculated in the following manner; height and width of the mould: average over 12 data points (6 in x and 6 in y direction); period of the mould: average period for 10 repeats (5 in x and 5 in y direction) for each array of structures. The same procedure was used to analyze AFM images of the imprinted polymer structures, however, instead of the width, the width at half height was used to determine the corresponding averages.

SIMS.[31] A time-of-flight secondary-ion mass (ToF-SIMS) spectrometer (ToF-SIMS IV, ION-TOF GmbH, Münster, Germany) equipped with a double stage reflection time-of-flight analyzer and a Bismuth cluster liquid-metal ion source was used. Spectra were recorded at a pressure of less than 5×10^{-9} mbar using the 25 keV Bismuth ion beam.

Contact Angle Measurements. The contact angles were measured on a contact angle microscope (Data Physis, OCA 15Plus or OCA 20) with Milli-Q water as the probe liquid. Advancing and receding contact angles were measured at room temperature.

Fluorescence and Optical Microscopy. Fluorescence microscopy images of dry samples on glass cover slips were recorded at room temperature on an Olympus IX 71 fluorescence microscope equipped with a U-MWG-2 fluorescent filter and a BA590 filterblock. Optical microscopy was performed using an Olympus BX 60.

Cell Work. Cell culture media and trypsin solution for cell dissociation were obtained from Lonza (Verviers, Belgium). Cell culture sera were bought from PAA Laboratories GmbH (Cölbe, Germany). All other reagents for cell culture work and cell fixation were from Sigma Aldrich GmbH (Taufkirchen, Germany) and the cell culture plastic material from Greiner (Frickenhausen, Germany). The human pancreatic carcinoma cell line PaTu8988S [36] was obtained from the Deutsche Sammlung von Mikroorganismen und Zellkulturen (DSMZ; Braunschweig, Germany). Cells were maintained under standard culture conditions in Dulbecco`s Modified Eagle`s Medium (DMEM), high glucose (4,5 g/l) and with L-glutamine (Lonza, Verviers, Belgium) supplemented with 5% Fetal Bovine Serum and 5% heat inactivated Horse Serum, (Invitrogen, Karlsruhe, Germany). For analysis of adherence cells were trypsinized, seeded sub confluent on manufactured substrates, cultured for 24 hrs and fixated with 1 % glutaraldehyde in PBS.[37] After PBS washing cell adherence was studied using light microscopy and AFM.

Results and Discussion

The patterning of PS_{690}-b-$PtBA_{1210}$ block copolymer films on glass by sequential nanoimprinting and i-μCP was investigated in detail to establish *(i)* an appropriate imprinting protocol to ensure faithful pattern transfer from the master to the films, *(ii)* full control of surface chemistry, *(iii)* optimized contact printing conditions to achieve maximized coverages of the transferred molecular species and *(iv)* to extend i-μCP to sub-micrometer pattern dimensions, which are difficult to achieve by μCP with conventional PDMS stamps.[38] Finally, (*v*) the functionality of the chemically patterned platforms as versatile biointerfaces was investigated.

The structure of the silicon / silicon nitride masters, which were fabricated using focused ion beam milling, could be successfully transferred to the PS_{690}-b-$PtBA_{1210}$ block copolymer films. Interferometric microscopy images (Figure 1a), as well as tapping mode atomic force microscopy images (Figure 1b), show the dimensions of the structures. These and different structures, also obtained by imprinting using conventional PDMS stamps as masters,[22] span feature sizes between >50 μm and 150 nm laterally and 1.50 μm and 18 nm vertically, respectively. Scanning electron microscopy images of other structures used are shown in the Supporting Information (Figure S-1).

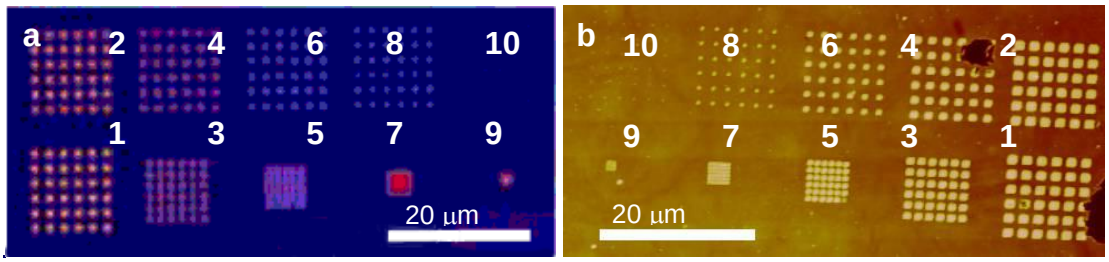

Figure 1. (a) Interferometer microscopy image of parts of the Si master (the numbers denote features with different dimensions). (b) AFM height image of a PS-b-PtBA film after imprinting with the master shown in panel (a). Feature sizes of the mould vary from 1.01 µm × 1.01 µm with an average height of 110 nm and a period of 2.0 µm (Figure 1a, structure 1) to 125 nm × 125 nm with an average height of 100 nm and a period of 250 nm (Figure 1a, structure 9). Feature sizes of the polymer replica vary from 1.07 µm × 1.07 µm with an average height of 102 nm and a period of 2.0 µm (Figure 1b, structure 1) to 153 nm × 153 nm with an average height of 80 nm and a period 250 nm (Figure 1b, structure 9).

Detailed analyses of the width, height and period of the mould and the imprinted block copolymer films were performed using tapping mode AFM. In Figure 2 typical data, as well as the analysis of all structures fabricated using the master shown in Figure 1a, are displayed (see also Figure S-2, Supporting Information). As can also be seen from the results plotted in Figures 2c and 2d, the heights and widths of the structures of the mould and the structured films are identical to within the experimental error. The polymer structures display slightly broader features, which can be attributed to AFM tip convolution effects.

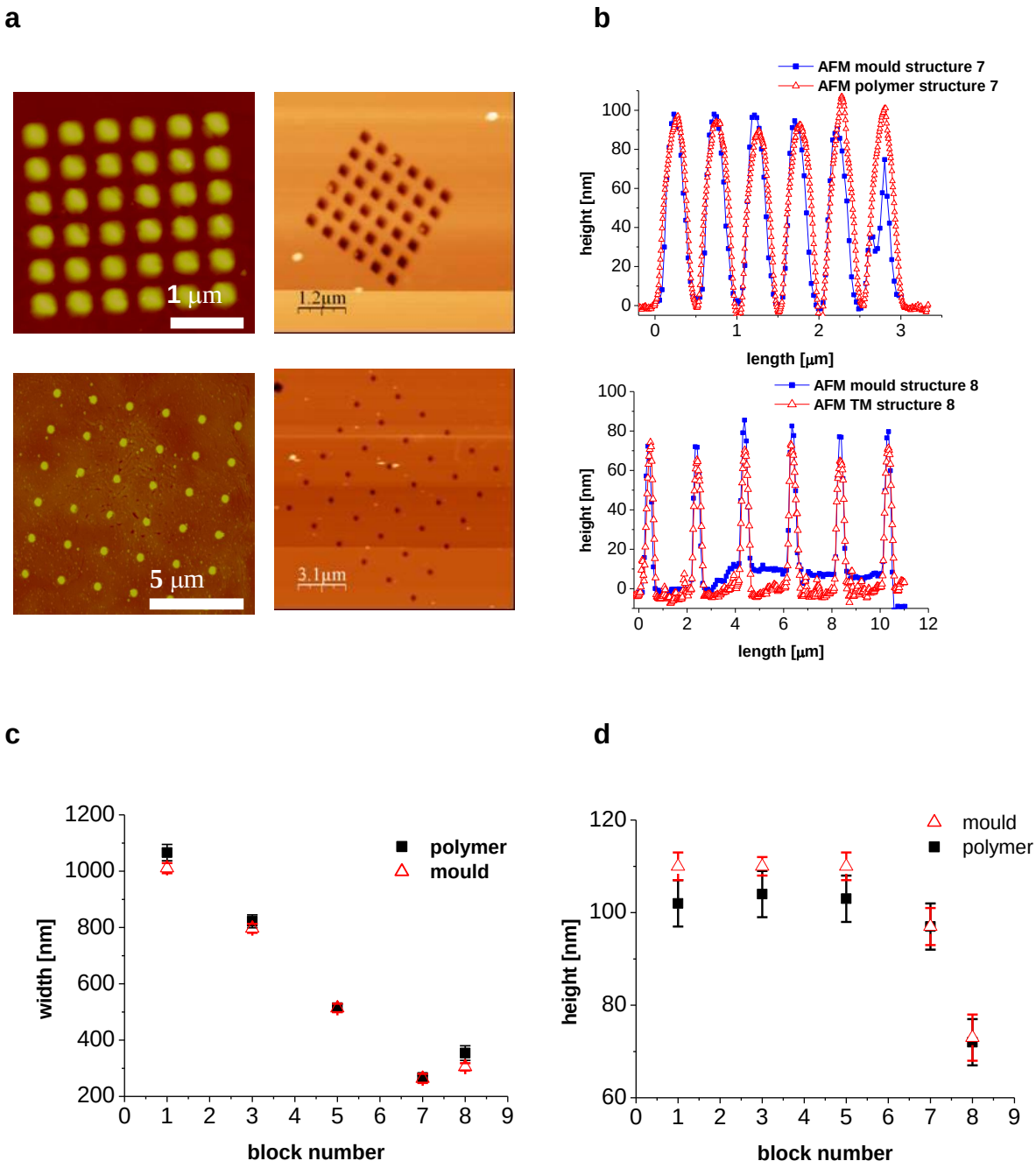

Figure 2. (a) AFM height images (z-scale: 200 nm (structure 7) and 100 nm (structure 8)) and (b) cross-sectional analyses comparing resulting polymer structures and moulds used. (c) and (d): Summary of heights and widths of the structures compared to the corresponding features in the mould, respectively.

The smallest structures present in the master (width: 125 nm; height: 100 nm with a period of 2.00 micrometers) did not reproduce as well as the larger features. Possibly the polymer adhered to the mould on the smaller samples, causing it to pull off.

The surface chemical composition of the imprinted films was found to be unaltered compared to the as-prepared films. Dynamic contact angle measurements, with water as a probe liquid, and ToF-SIMS showed, to within the experimental error, identical contact angles (advancing CA of 90 º and receding CA 79 º) and ToF-SIMS data, respectively (Tables S-1, S-2 and Figure S-3, Supporting Information). In particular, the mass fragments detected and identified for the negative polarity mode show evidence for the presence of the polymer backbone and t-butyl ester groups in the analyzed surface region. The absence of peaks that can be unequivocally attributed to the aromatic ring in PS and the absence of other PS-specific fragments thus lead to the conclusion that the surface is poor in PS in the sampled depth of < 5 nm. These observations confirm the previously reported finding of an ~ 8 nm thick PtBA skin layer on these films as determined by angle-dependent X-ray photoelectron spectroscopy.[28a]

In addition, these results are in agreement with the literature on the thermal stability of PS and PtBA. The block copolymer stays intact as the temperatures used for imprinting (100°C) are well below the reported threshold for thermal degradation of PS (~ 400°C) and for the elimination of isobutylene and the concomitant formation of poly(acrylic acid) and subsequently poly(acrylic acid anhydride) observed at T > 200°C, respectively.[39] Independent thermal gravimetric analysis (TGA) and Fourier transform infrared spectroscopy experiments on the PS_{690}-b-$PtBA_{1210}$ material used in this study confirmed an on-set temperature for the mentioned chemical transformation of the PtBA block of ~ 220°C.[40] In addition to the absence of chemical reactions in the

topmost region of the structured films, we can also exclude the presence of organic contaminations that may hinder subsequent derivatization reactions according to previously published procedures. However, traces of sodium and calcium-containing contaminations were found in depth-resolved ToF-SIMS spectra (see Supporting Information, Figure S-4).

The CA and SIMS data thus indicate that the PtBA skin layer is not affected by the topographic patterning. Therefore, the previously applied hydrolysis under acidic conditions and the activation with EDC / NHS, for the subsequent covalent attachment of primary amines can be successfully carried out on the imprinted films as well.[28,29] However, before discussing patterns of proteins and PEG fabricated by i-μCP, the optimized transfer of molecules using an oxidized PDMS stamp is presented.

For the i-μCP approach reported by the Textor group, utilizing the PLL-PEG adsorbate system,[24] repeated printing steps were required to achieve acceptable coverages of the adsorbate to suppress undesired non-specific protein adsorption.[22] The PLL-PEG coatings are typically applied to oxide surfaces by dip-coating from solution, while the μCP processes occur in the absence of liquid in the conformal contact formed between the elastomeric stamp and the sample surface. Since the functionalization of the PS_{690}-b-$PtBA_{1210}$ platform used here relies on covalent attachment and not multi-site physisorption, one may expect differences regarding the printing time due to the different kinetics of the relevant processes.

In Figure 3, the thickness of grafted PEG-NH_2 layers determined by ellipsometry is shown for different molar masses of PEG-NH_2 and different printing times (Figure 3a), as well as for PEG_{5000}-NH_2 for different printing methods (Figures 3b and 3c). Here shorter stamp-film contact times and a subsequent post-printing cure period were applied before rinsing (T = 25 ± 3 ^{o}C, t = 180 s, 300 s and 3 hours respectively, cure

period 3 hours). In addition, the deposition of an excess of PEG on the oxidized stamp surface was investigated (Figure 3c). For these latter experiments featureless stamps were used on non-structured block copolymer films to simulate the reaction conditions for the reaction that was later carried out in micro- and nanocontacts (see below).

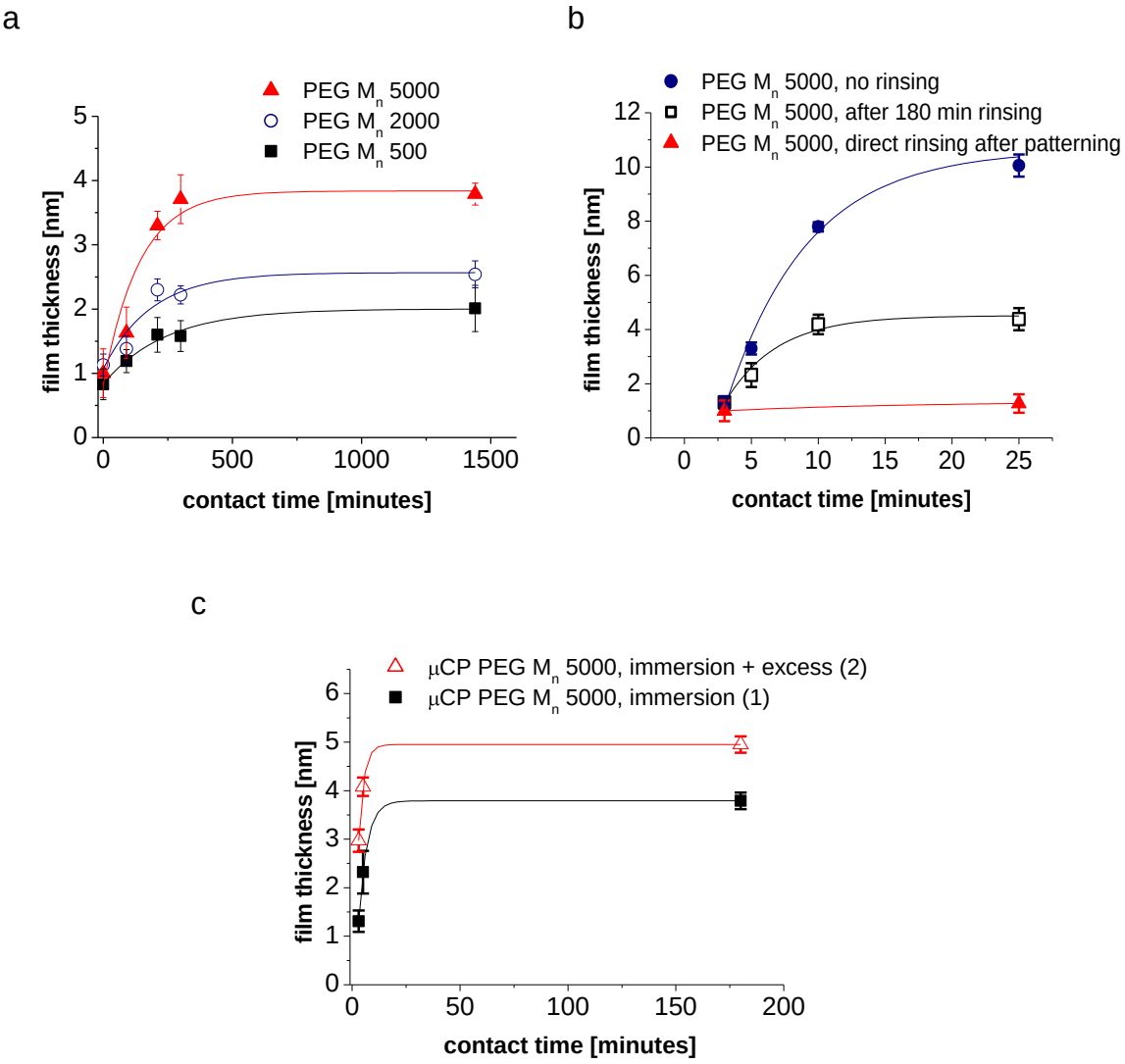

Figure 3. (a) Values of dry ellipsometric thickness of grafted PEG layers for different stamp-film contact time and molar masses. (b) Comparison of values of transferred and grafted film thickness of PEG_{5000} for the specified conditions. (c) Comparison of values of grafted film thickness for different stamp loading conditions: 1. Immersion of the PDMS stamp in PEG solution for 1 hour; 2. Same procedure but with excess of PEG on top of the stamp after 1 hour immersion (ellipsometry was performed after waiting

for > 180 minutes before rinsing with PBS and drying) for PEG_{5000}. In both cases stamps were loaded by a 1.0 x 10^{-4} M solution of PEG in PB buffer either by only immersion (1), or by immersion and subsequent application of excess solution (2). The lines represent exponential fits and serve as a guide for the eye.

The highest grafting densities in conventional printing were observed for stamp-film contact times in excess of 3 - 4 hours (Figure 3a). These long printing times are certainly not economical and are orders of magnitude longer than the ones used in μCP of thiols on gold[13] or PLL-PEG onto structured PS.[22] This observation may be in part attributed to the fact that PEG is a telechelic polymer and is covalently attached via its chain terminus. Hence the diffusion of the chain end to reactive NHS ester sites on the activated film surface may be responsible for the observed slow kinetics. Similarly, the coverage of PEG on the oxidized stamp may be too low to ensure a steep enough concentration gradient.

A comparison of Figure 3a and Figure 3b shows that the thickness of the transferred (but not immobilized) film increased exponentially with stamp-film contact time. In addition, the transferred layer is significantly thicker than the grafted, i.e. covalently attached PEG (the data for PEG_{500}-NH_2 and PEG_{2000}-NH_2 are shown in Figure S-5 in the Supporting Information). Furthermore, the value of the thickness of the grafted PEG_{5000} after 10 minutes printing followed by a 180 minute post-printing cure period before rinsing is comparable to the thickness value obtained by 180 to 240 minute stamp-film contact time followed immediately by rinsing. These observations are fully in line with a post-contact grafting reaction that goes to completion over the mentioned time scale.

Since the value of the thickness of the transferred film (prior to rinsing, see Figure 3b) depends on the printing time under these conditions, its value may be increased by increasing the loading of PEG on the stamp. Enhanced stamp loading may consequently lead to the formation of thicker non-bound PEG film that serves as a reservoir for diffusion of chains from the film surface into the near-surface region of the film.[28] Indeed, as shown in Figure 3c, if an excess of PEG_{5000}-NH_2 is deposited on the stamp (as compared to soaking the stamp in a dilute PEG solution for 1 hour), an increased thickness of the *grafted* PEG layer can be achieved.[29] This thickness is significantly larger than that obtained by wet chemical grafting methods and indicates that the high local concentration (and pressure) under solvent-less conditions of μCP improve the coupling efficiency.[41] The thus obtained higher grafting densities are linked to improved performance in the suppression of non-specific protein adsorption.[42]

With the optimized printing protocol at hand, the topographically structured block copolymer films were activated and functionalized in an identical manner. Using optical microscopy, it was ensured that the featureless stamp and the structured polymer film were indeed in conformal contact (Figure 4a). Dye-labeled BSA transferred to and covalently immobilized on the NHS activated PS_{690}-b-$PtBA_{1210}$ film was visualized in fluorescence microscopy images (Figure 4b). Faithful transfer to the contacting top part of the structures and the absence of cross-contamination were observed.

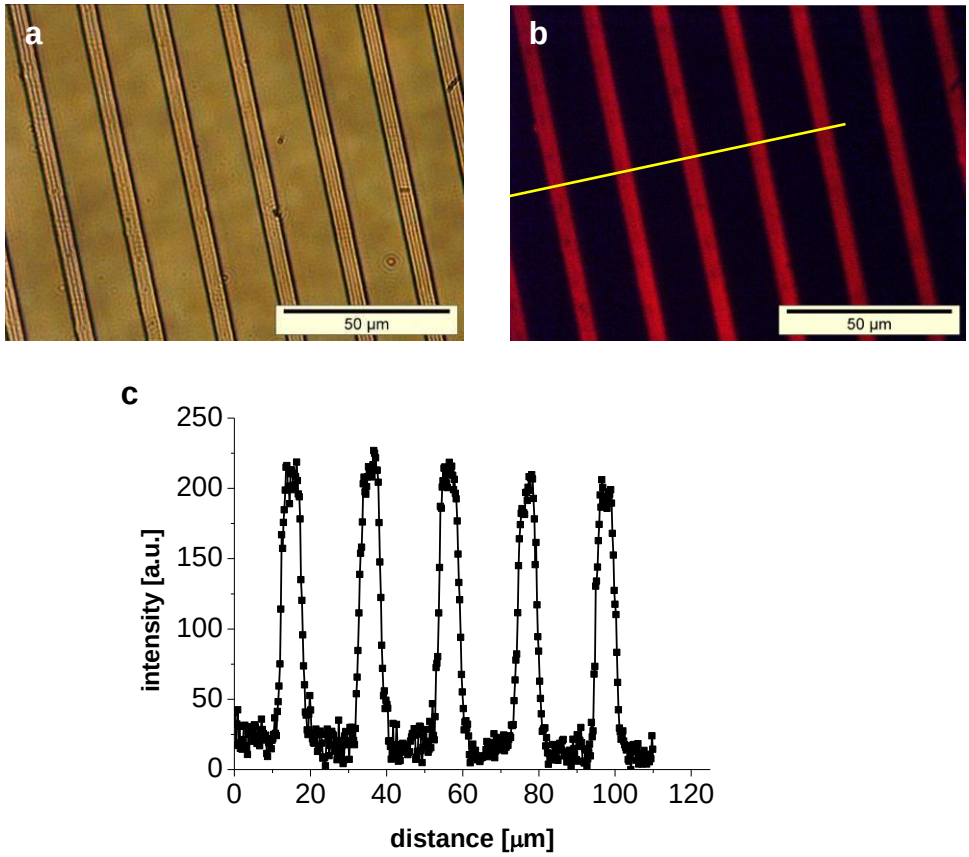

Figure 4. (a) Optical microscopy image of PDMS stamp in contact with PS_{690}*-b-*$PtBA_{1210}$ *film on glass taken in transmission mode. (b) Corresponding fluorescence microscopy image, acquired after the stamp was removed, showing the fluorescence emission of dye-labeled BSA that has been transferred from the stamp to the structured polymer film in the areas of conformal contact. (c) Cross-sectional plot of data shown in panel (b).*

This process worked efficiently for different pattern geometries and sizes to below 1.0 micrometer (Figures 5 and 6).

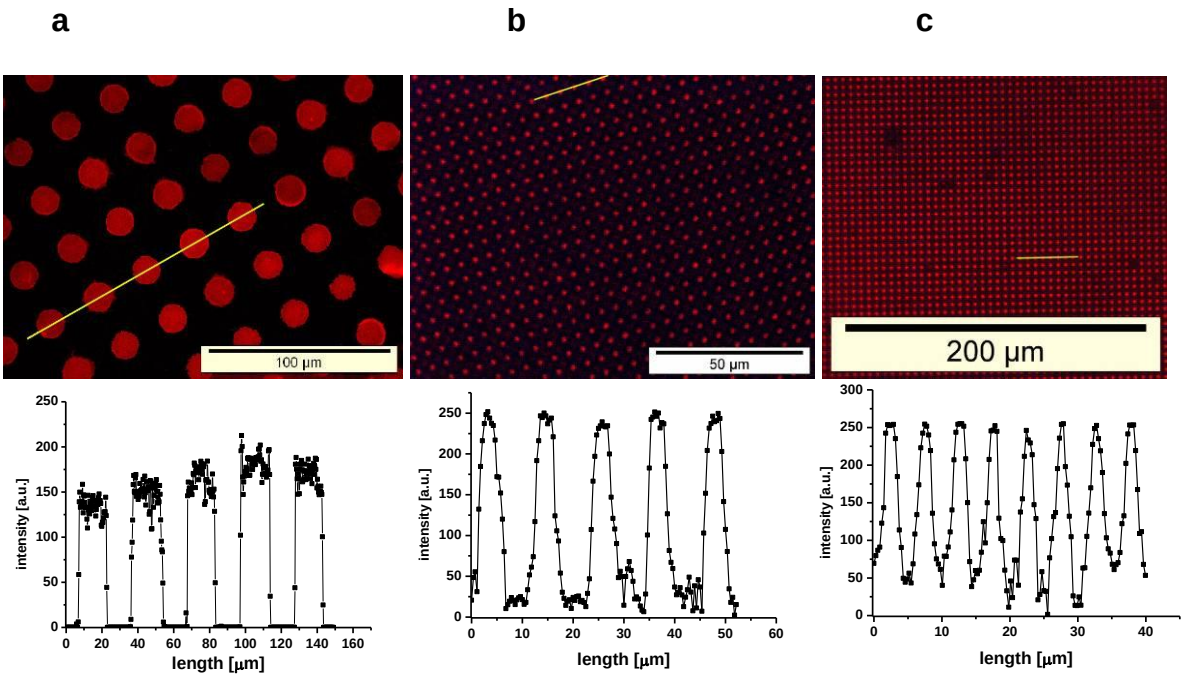

Figure 5. Fluorescence microscopy images (top) and fluorescence intensity cross sectional plots (bottom) of micropatterns of BSA on PS_{690}-b-$PtBA_{1210}$ block copolymer thin films.

The fluorescence microscopy images in Figure 5 show that BSA was transferred selectively to the top part of the imprinted features of the block copolymer films. The coverages of the protein on neighboring spot-like features is homogeneous as judged from the only small variations in the corresponding fluorescence emission intensity. Missing features in Figure 5c are attributed to defects in the underlying polymer film as a consequence of defects in the master or an incomplete pattern transfer in the imprinting step. The scalability of the process on length scales covering the 15 to 2.5 µm range is thus clearly demonstrated.

These length scales for chemical patterning are in principle accessible by conventional µCP[13,14] on various supports and reactive µCP[27] on similar polymer platforms. However, using suitable topographically structured films the approach can be extended to the sub-micrometer range combining topographic and chemical

patterning. In the AFM force-volume images shown in Figure 6,[43,44] the successful modification of the imprinted film (500 nm wide lines) with BSA is evident. Compared to the surrounding matrix of unmodified NHS ester terminated polymer, the BSA-functionalized elevated ridges show reduced adhesive forces (corresponding to bright contrast in the FV image). For more narrowly spaced features the position-resolved analysis becomes challenging even with AFM. The adhesive forces may show side wall effects (tip imaging), thus no precise mapping near elevated structures (lines or posts) is possible.

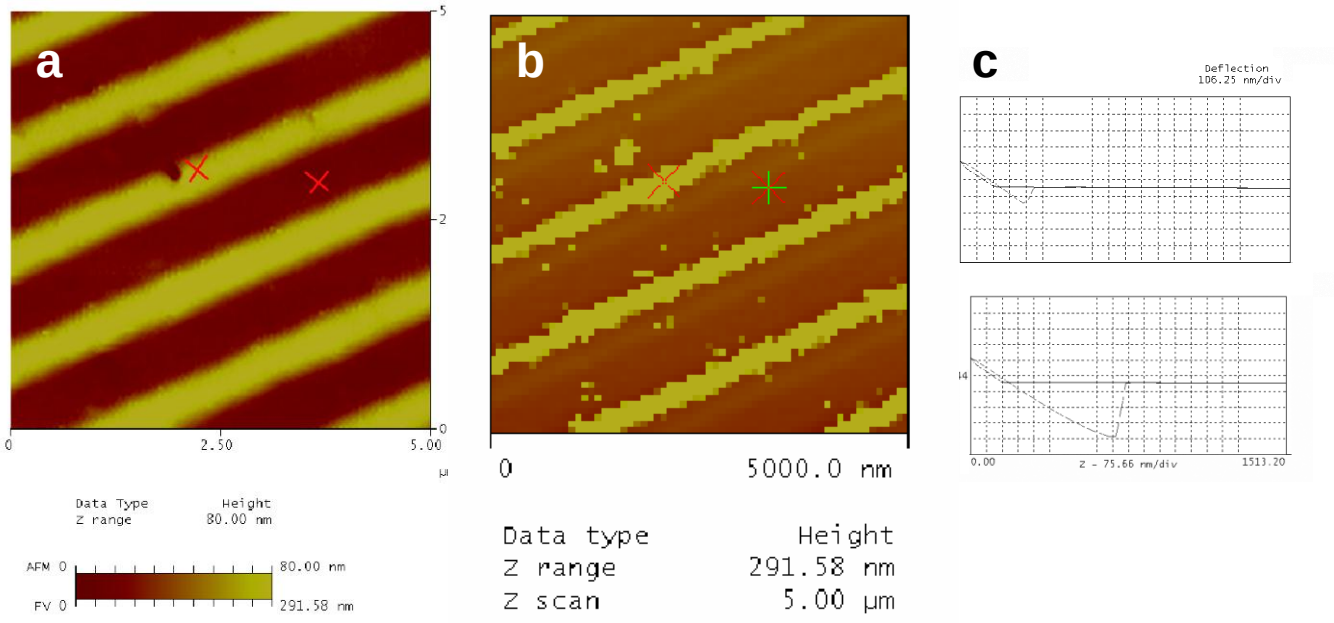

Figure 6. (a) Force volume height and (b) corresponding force image of BSA transferred to the polymer structure by i-μCP. In panel (c) two representative force displacement curves are displayed that clearly show the different pull-off forces between BSA covered mesas (~ 9 nN) and NHS-functionalized flat areas of the film (~ 32 nN).[44]

We can conclude at this point that i-μCP is a useful (soft) lithographic technique that can be applied in conjunction with optimized robust polymer platforms to fabricate topographically structured and (bio)-chemically patterned functional interfacial architectures.[45] One can control pattern size and spacing over a large range and some of the restrictions of conventional μCP using soft elastomeric stamps, such as stamp feature deformation and collapse, are overcome. The aspect ratio of the topographic structures can be increased relative to PDMS, we note however, that the so-called roof collapse is not eliminated at extreme stamp feature separations.

The functionality of the topographically structured and chemically patterned biointerfaces was confirmed in studies with pancreatic cancer cells. Functionality refers to *(i)* the implementation of anti-biofouling functionality and *(ii)* the immobilization of proteins (e.g. fibronectin) and other relevant biomolecules in their functional form.

Pancreatic adenocarcinomas are highly invasive tumors forming metastases early in tumor development. Tumor growth and invasion is promoted by a tumor microenvironment mainly composed of host epithelial cells, stromal fibroblast and extracellular matrix proteins.[46] Fibronectin is known to be upregulated in pancreatic tumors, to increase tumor cell survival, and to promote tumor proliferation and metastasis by cytokine mediated pathways.[47] The here used PaTu8988S cells are characterized by a nonpolar organization of the cell cytoplasma and tumor growth in a nude mouse model.[36] PaTu8988S cells express fibronectin binding integrin subunits and bind to fibronectin coated surfaces.[48]

By imprint lithography and subsequent i-μCP substrates were fabricated that exposed fibronectin on top of 5 μm wide (850 nm high) lines that were separated by PEG_{5000}-passivated flat areas (spacing: 15 μm). Using optical microscopy and TM-AFM, cells were observed to attach preferentially at and spread out along the 5 μm

wide, fibronectin-covered mesas of the structure (Figure 8). The PEG-ylated areas in between the lines were avoided. Similar observations were made on BSA - PEG_{5000} functionalized substrates with identical dimensions, while on exclusively topographically structured, non-functionalized samples cells attached without preference on top and between the structures (no data shown). These data thus provide convincing evidence for the functionality of the simultaneously topographically and chemically micro- and nanostructured and -patterned platforms and validate the entire approach.

a b

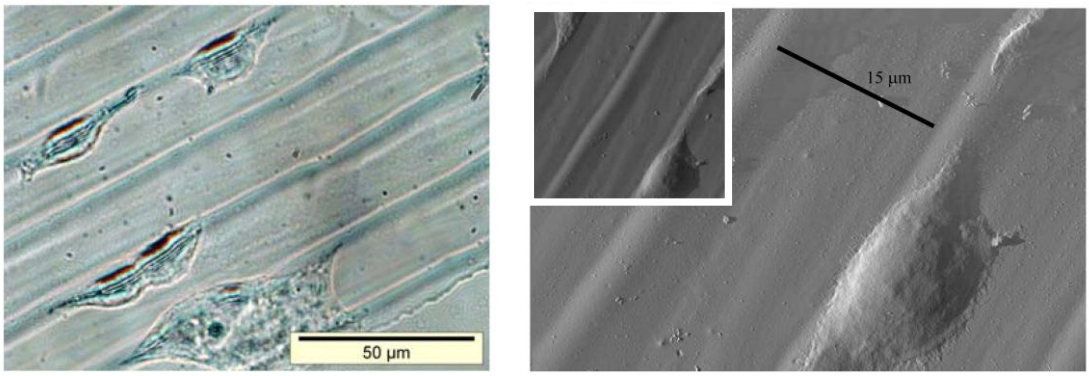

Figure 8. (a) Optical microscopy and (b) TM-AFM phase images of fixated PaTu8988S cells on topographically structured and chemically patterned substrate reveal the preferential attachment on the 5 µm wide fibronectin-functionalized mesas (line spacing for all images: 15 µm).

Conclusions

In this paper we have shown that inverted microcontact printing on spin-coated films of polystyrene-block-poly(*tert*-butyl acrylate) provides a versatile approach for the fabrication of patterned biointerfaces across the length scales, from tens of micrometers down to 150 nanometers. In particular, the fabrication of patterns comprising small spot sizes with large spacings is feasible by printing reactants using a featureless elastomeric stamp onto a topographically structured reactive polymer film. Due to the glassy PS blocks and the robust covalent amide linkages, the derivatized films showed excellent stability under a broad range of processing conditions. This i-μCP strategy hence provides access to versatile biointerfaces and platforms, as shown for the interaction of PaTu8988S cells with topographically and chemically structured surfaces.

Acknowledgment

The authors would like to thank Jordi Toset (AFM), M-J. Lopez Bosque (FIB/SEM), and R. Diez (ToF-SIMS) at the Barcelona Science Park, and T. Wahlbrink and C. Moorman at AMO Gesellschaft für Angewandte Mikro- und Optoelektronik GmbH, Germany (moulds). The support of the EU (NoE Nano2Life, "Maptech" Marie Curie grant (ML)) and the Spanish Ministry of Science and Education (MEC) (Ramon y Cajal grant (CAM)) is gratefully acknowledged. This work has been financially supported by the BMBF (grant to JS), the MESA$^+$ Institute for Nanotechnology of the University of Twente, the Council for Chemical Sciences of the Netherlands Organization for Scientific Research (CW-NWO), also in the framework of the *vernieuwingsimpuls* program (grant awarded to HS).

Supporting Information Available: Detailed experimental procedures, SEM images of moulds, AFM analyses of imprints, ToF-SIMS spectra of polymer films, ToF-SIMS depth analysis, ellipsometry data for PEG-500 and PEG-2000, fluorescence microscopy data for simultaneously patterned films and tabulated contact angle and ToF-SIMS data incl. peak assignment. This material is available free of charge via the Internet at http://pubs.acs.org.

References

1 (a) Fodor, S. P. A.; Read, J. L.; Pirrung, M. C.; Stryer, L.; Lu, A. T; Solas, D. *Science* **1991**, *251*, 767-773. (b) Pirrung, M. C. *Angew. Chem. Int. Ed*. **2002**, *41*, 1277-1289.

2 (a) Lockhart, D. J.; Winzeler, E. A. *Nature* **2000**, *405*, 827-836. (b) Camarero, J. A.; Kwon, Y; Coleman, M. A. *J. Am. Chem. Soc.* **2004**, *126*, 14730-14731. (c) Lynn, D. J.; Freeman, A. R.; Murray, C; Bradley, D. G. *Genetics* **2005,** *170*, 1189-1196.

3 (a) Mrksich, M. *Chem. Soc. Rev*. **2000**, *29*, 267-273. (b) Mrksich, M. *Curr. Opin. Chem.Biology* **2002**, *6*, 794-797. (c) Chen, C. S.; Jiang, X.; Whitesides, G. M. *MRS Bull.* **2005**, *30*, 194-201.

4 (a) Blau, H. M.; Baltimore, D. J. *J. Cell Biol.* **1991**, *112*, 781-783. Ruoslahti, E.; Obrink B. *Exp. Cell Res.* **1996**, *227*, 1-11. (b) Cameron, J.; Wilson, B. E.; Clegg, R. E.; Leavesley, D. I.; Pearcy, M. *J. Tissue Engin.* **2005**, *11*, 1-2.

5 (a) Chen, C. S.; Mrksich, M.; Huang, S.; Whitesides, G. M.; Ingber, D. E.; *Science* **1997**, *276*, 1425-1428. (b) Curtis, A.; Wilkinson, C. *Biomaterials* **1997**, *18*, 1573-1583. (c) Pelham, R. J.; Wang, Y.-L. *Proc. Natl. Acad. Sci. USA* **1997**, *94*, 13661. (d) Curtis, A. S.; Casey, B.; Gallagher, J. O.; Pasqui, D.; Wood, M. A.; Wilkinson, C. D. *Biophys. Chem.* **2001**, *94*, 275-283. (e) Curtis, A. S.; Gadegaard, N.; Dalby, M. J.; Riehle, M. O.; Wilkinson, C. D.; Aitchison G.; *IEEE Trans Nanobiosci.* **2004**, *3*, 61-65. (f) Dalby, M. J.; Silvio, L. D.; Harper, E. J.; Bonfield, W. *J. Mater. Sci. Mater. Med.* **2002**, *13*, 311-314. (g) Ingber, D. E. *J. Cell Sci.* **2003**, *116*, 1157-1173. (h) Ingber, D. E. *J. Cell Sci.* **2003**, *116*, 1397-1408.

6 (a) Bray, D.; Levin, M. D.; Morton-Firth, C. J. *Nature* **1998**, *393*, 85-88. (b) Germain, R. N. *Current Biology* **1997**, *7*, R640-R644. (c) Willmann, R; Fuhrer, C. *Cell. Mol. Life Sci.* **2002**, *59*, 1296-1316.

7 (a) Arnold, M.; Cavalcanti-Adam, E.; Glass, R.; Blümmel, J.; Eck, W.; Kanthlener, M.; Kessler, H.; Spatz, J. P. *ChemPhysChem* **2004**, *5*, 383-388. (b) Cavalcanti-Adam, E.; Micoulet, A.; Blümmel, J.; Auernheimer, J.; Kessler, H.; Spatz, J. P. *Europ. J. Cell Biol.* **2006**, *85*, 219-224.

8 (a) Maheshwari, G.; Brown, G.; Lauffenburger, D. A.; Wells, A.; Griffith, L. G. *J. Cell Sci.* **2000**, *113*, 1677-1686. (b) Koo, L. Y.; Irvine, D. J.; Mayes, A. M.; Lauffenburger, D. A; Griffith L.G. *J. Cell Sci.* **2002**, *115*, 1423-1433.

9 (a) Horbett, T. A. *Coll. Surf. B* **1994**, *2*, 225-240 (b) Siebers, M. C.; ter Brugge, P. J.; Walboomers, X. F.; Jansen J. A. *Biomaterials* **2005**, *26*, 137-146.

10 Falconnet, D.; Csucs, G.; Grandin, H. M.; Textor M. *Biomaterials* **2006**, *27*, 3044-3063.

11 Kasemo, B. *Surf. Sci;* **2002,** *500*, 656-677.

12 Pease, A. C.; Solas, D.; Sullivan, E. J.; Cronin, M. T.; Holmes, C. P.; Fodor, S. P. A. *Proc. Natl. Acad. Sci. USA* **1994**, *91*, 5022-5026.

13 Kumar, A.; Whitesides, G. M. *Appl. Phys. Lett*. **1993**, *63*, 2002-2004.

14 (a) Bernard, A.; Renault, J. P.; Michel, B.; Bosshard, H. R.; Delamarche, E. *Adv. Mater*. **2000**, *12*, 1067-1070. (b) Falconnet, D.; Koenig, A.; Assi, T.; Textor M. *Adv. Func. Mater*. **2004**, *14*, 749-756.

15 (a) Guo, L. J. *J. Phys. D Appl. Phys.* **2004**, *37*, R123-R141. (b) Charest, J. L.; Bryant, L. E.; Garcia, A. J.; King, W. P. *Biomaterials* **2004**, *25*, 4767-4775.

16 (a) Xia, Y.; Whitesides, G. M. *Angew. Chem., Int. Ed.* **1998**, *37*, 550-575. (b) Gates, B. D.; Xu, Q.; Stewart, M.; Ryan, D.; Willson, C. G.; Whitesides, G. M. *Chem. Rev.* **2005**, *105*, 1171-1196.

17 Inerowicz, H. D.; Howell, S.; Regnier, F. E.; Reifenberger, R. *Langmuir* **2002**, *18*, 5263-5268.

18 (a) Lauer, L.; Klein, C.; Offenhausser, A. *Biomaterials* **2001**, *22*, 1925-1932. (b) Roca-Cusachs, P.; Rico, F.; Martínez, E.; Toset, J.; Farré, R.; Navajas, D. *Langmuir* **2005**, *21*, 5542-5548. (c) Bietsch, A.; Michel B. *J. Appl. Phys.* **2000**, *88,*, 4310-4318. (d) Delamarche, E.; Schmid, H.; Michel, B., Biebuyck, H. *Adv. Mater.* **1997**, *9*, 741-746.

19 Bessueille, F.; Pla-Roca, M.; Mills, C. A.; Martinez, E.; Samitier, J.; Errachid, A. *Langmuir* **2005,** *21*, 12060-12063.

20 Libioulle, L.; Bietsch, A.; Schmid, H.; Michel, B.; Delamarche, E. *Langmuir* **1999**, *15*, 300-304.

21 Delamarche, E.; Schmid, H.; Bietsch, A.; Larsen, N. B.; Rothuizen, H.; Michel, B.; Biebuyck, H. *J. Phys. Chem. B* **1998**, *102*, 3324-3334.

22 Dusseiller, M. R.; Schlaepfer, D.; Koch, M.; Kroschewski, R.; Textor, M. *Biomaterials* **2005**, *26*, 5917-5925.

23 Sharpe, R. B. A.; Burdinski, D.; Huskens, J.; Zandvliet, H. J. W.; Reinhoudt, D. N.; Poelsema, B. *J. Am. Chem. Soc*. **2005,** *127*, 10344-10349.

24 Kenausis, G. L.; Voros, J.; Elbert, D. L.; Huang, N. P.; Hofer, R.; Ruiz-Taylor, L.; Textor, M.; Hubbell, J. A.; Spencer, N. D. *J. Phys. Chem.* **2000**, *104*, 3298-3309.

25 Charest, J. L.; Eliason, M. T.; García, A. J.; King, W. P.; Talin, A. A.; Simmons, B.A. *J. Vac. Sci. Technol., B.* **2005**, *23*, 3011-3014.

26 Soolaman, D. M.; Yu, H-Z. *J. Phys. Chem. C* **2007**, *111*, 14157-14164.

27 (a) Feng, C. L.; Vancso, G. J.; Schönherr, H. *Adv. Funct. Mater.* **2006**, *16*, 1306-1312. (b) Feng, C. L.; Embrechts, A.; Vancso, G. J.; Schönherr, H. *Europ. Polym. J.* **2006**, *42*, 1954-1965. (c) Feng, C. L.; Vancso, G. J.; Schönherr, H. *Langmuir* **2007,** *23*, 1131-1140.

28 (a) Feng, C. L.; Vancso, G. J.; Schönherr, H. *Langmuir* **2005**, *21*, 2356. (b) Feng, C. L.; Embrechts, A.; Bredebusch, I.; Bouma, A.; Schnekenburger, J.; García-Parajó, M.; Domschke, W.; Vancso, G. J.; Schönherr, H. *Europ. Polym. J.* **2007,** *43*, 2177-2190.

29 Feng, C. L.; Embrechts, A.; Bredebusch, I.; Schnekenburger, J.; Domschke, W.; Vancso, G. J.; Schönherr, H. *Adv. Mater.* **2007**, *19*, 286-290.

30 Feng, C. L.; Zhang, Z.; Förch, R.; Knoll, W.; Vancso, G. J.; Schönherr, H. *Biomacromolecules* **2005**, *6*, 3243-3251.

31 The detailed procedures for mould fabrication, imprint lithography, AFM and SIMS analysis are included in the supporting information.

32 Mills, C. A.; Martinez, E.; Bessueille, F.; Villanueva, G.; Bausells, J.; Samitier, J.; Errachid, A. *Microelectronic Engineering* **2005**, *78-79*, 695-700.

33 Hillborg, H.; Tomczak, N.; Olah, A.; Schönherr, H.; Vancso, G. J. *Langmuir* **2004**, *20*, 785-794.

34 *Polymer Handbook*, 3rd ed. Brandrup, J.; Immergut, E. H. John Wiley & Sons: New York, **1989**.

35 (a) Levenberg, K. *Quart. Appl. Math.* **1944**, *2*, 164-168 (b) Marquardt, D. *SIAM J. Appl. Math.* **1963**, *11*, 431-441 (c) Gill, P. E.; Murray, W. *SIAM J. Numer. Anal.* **1978**, *15*, 977-992.

36 Elsasser, H. P.; Lehr, U.; Agricola, B.; Kern, H. F. *Virchows Arch. B Cell Pathol. Incl. Mo.l Pathol.* **1992**, *61*, 295-306.

37 Kemper, B.; Carl, D.; Schnekenburger, J.; Bredebusch, I.; Schafer, M.; Domschke, W.; von Bally, G. *J. Biomed. Opt*. **2006**, *11*, 34005.

38 Stiffened stamps for high resolution printing have been reported: (a) Schmid, H.; Michel, B. *Macromolecules* **2000**, *33*, 3042-3049. (b) Odom, T. W.; Love, J. C.; Wolfe, D. B.; Paul, K. E.; Whitesides, G. M. *Langmuir* **2002**, *18*, 5314-5320.

39 La, Y. H.; Edwards, E. W.; Park, S. M.; Nealey, P. F. *Nano Lett.* **2005**, *5*, 1379-1384.

40 Duvigneau, J.; Schönherr, H.; Vancso, G. J. *unpublished data.*

41 Sullivan, T. P.; van Poll, M. L.; Dankers, P. Y. W.; Huck, W. T. S. *Angew. Chem Int. Ed.* **2004**, *43*, 4190-4193.

42 Michel, R.; Pasche, S.; Textor, M.; Castner, D. G. *Langmuir* **2005**, *21*, 12327-12332.

43 Schönherr, H.; Feng, C. L.; Tomczak, N.; Vancso, G. J. *Macromol. Symp.* **2005**, *230*, 149-157.

44 Vancso, G. J.; Hillborg, H.; Schönherr, H. *Adv. Polym. Sci.* **2005**, *182*, 55-129.

45 As shown in the Supporting Information (Figure S-6), the transfer of BSA and the passivation of the non-contacted areas of the NHS-activated polymer film with grafted PEG were carried out *simultaneously*. In a sandwich structure of film and stamp, channels were formed that were filled with PEG-containing buffer solution by capillary action. At the same time, BSA was transferred and covalently bound to the film in the conformal contact areas between BSA-

covered featureless stamp and the topographically structured film, while inside the channels PEG was grafted as a layer to reduce non-specific adsorption.

46 Mahadevan, D.; von Hoff, D. D. *Mol. Cancer Ther*. 2007, *6*, 1186-1197.

47 (a) Vaquero, E. C.; Edderkaoui, M.; Nam, K. J.; Gukovsky, I.; Pandol, S. J.; Gukovskaya, A. S. *Gastroenterology* **2003**, *125*, 1188-1202. (b) Lowrie, A. G.; Salter, D. M.; Ross, J. A. *Br. J. Cancer* **2004**, *91*, 1327-1334

48 Vogelmann, R.; Kreuser, E. D.; Adler, G.; Lutz, M. P. *Int. J. Cancer* **1999**, *80*, 5, 791-795

Published in: Langmuir 24:16 (2008) 8841-8849

For Table of Contents Use Only

Inverted Microcontact Printing on Polystyrene-block-Poly(tert-butyl acrylate) Films: A Versatile Approach to Fabricate Structured Biointerfaces Across the Length Scales

Anika Embrechts, Chuan Liang Feng, Christopher A. Mills, Michael Lee, Ilona Bredebusch, Jürgen Schnekenburger, Wolfram Domschke, G. Julius Vancso, and Holger Schönherr*